The Journal of Chemical Physics

RESEARCH ARTICLE | OCTOBER 04 2023

ManyHF-based full-dimensional potential energy surface development and quasi-classical dynamics for the Cl + CH_3NH_2 reaction FREE

Tímea Szűcs ; Gábor Czakó

J. Chem. Phys. 159, 134306 (2023)
https://doi.org/10.1063/5.0166680

Articles You May Be Interested In

ManyHF: A pragmatic automated method of finding lower-energy Hartree–Fock solutions for potential energy surface development

J. Chem. Phys. (February 2022)

Ion imaging study of reaction dynamics in the $N^+ + CH_4$ system

J. Chem. Phys. (October 2012)

Photodissociation dynamics of methylamine in the blue edge of the *A*-band. I. The H-atom elimination channel

J. Chem. Phys. (June 2023)

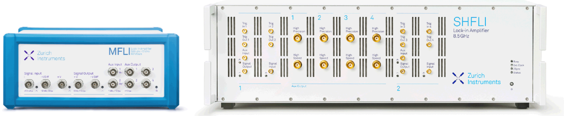

AIP Publishing

The Journal of Chemical Physics | ARTICLE | pubs.aip.org/aip/jcp

ManyHF-based full-dimensional potential energy surface development and quasi-classical dynamics for the Cl + CH_3NH_2 reaction

Cite as: J. Chem. Phys. 159, 134306 (2023); doi: 10.1063/5.0166680
Submitted: 6 July 2023 • Accepted: 6 September 2023 •
Published Online: 4 October 2023

Tímea Szűcs and Gábor Czakó[a)]

AFFILIATIONS

MTA-SZTE Lendület Computational Reaction Dynamics Research Group, Interdisciplinary Excellence Centre
and Department of Physical Chemistry and Materials Science, Institute of Chemistry, University of Szeged,
Rerrich Béla tér 1, Szeged H-6720, Hungary

[a)]**Author to whom correspondence should be addressed:** gczako@chem.u-szeged.hu

ABSTRACT

A full-dimensional spin–orbit (SO)-corrected potential energy surface (PES) is developed for the Cl + CH_3NH_2 multi-channel system. Using the new PES, a comprehensive reaction dynamics investigation is performed for the most reactive hydrogen-abstraction reactions forming HCl + CH_2NH_2/CH_3NH. Hartree–Fock (HF) convergence problems in the reactant region are handled by the ManyHF method, which finds the lowest-energy HF solution considering several different initial guess orbitals. The PES development is carried out with the ROBOSURFER program package, which iteratively improves the surface. Energy points are computed at the ManyHF-UCCSD(T)-F12a/cc-pVDZ-F12 level of theory combined with basis set (ManyHF-RMP2-F12/cc-pVTZ-F12 − ManyHF-RMP2-F12/cc-pVDZ-F12) and SO (MRCI+Q/aug-cc-pwCVDZ) corrections. Quasi-classical trajectory simulations show that the CH_3-side hydrogen abstraction occurs more frequently in contrast to the NH_2-side reaction. In both cases, the integral cross sections decrease with increasing collision energy (E_{coll}). A reaction mechanism shifting from indirect to direct stripping can be observed from the opacity functions, scattering angle, and translation energy distributions as E_{coll} increases. Initial attack angle distributions reveal that chlorine prefers to abstract hydrogen from the approached functional group. The collision-energy dependence of the product energy distributions shows that the initial translational energy mainly transfers to product recoil. The HCl vibrational and rotational energy values are comparable and nearly independent of collision energy, while the CH_2NH_2 and CH_3NH co-products' vibrational energy values are higher than the rotational energy values with more significant E_{coll} dependence. The HCl($v = 0$) rotational distributions are compared with experiment, setting the direction for future investigations.

I. INTRODUCTION

In 2004, a comprehensive review was reported on the dynamics of chlorine-atom reactions with organic molecules, such as methane, ethane, methanol, methylamine, methyl-halides, etc.[1] The scattering dynamics of the above systems were probed experimentally, providing vibrationally resolved rotational distributions for the HCl product as well as angular distributions.[1–5] The accurate simulation of these measured quantities has challenged theory for many years.[6–12] In experiment, the size of the organic molecule does not complicate the detection of the HCl product obtained by hydrogen abstraction from the molecule with the Cl atom. However, theory has to fight against the dimensionality problem, which increases with the number of atoms. Therefore, in the 2000s, accurate dynamics simulations were only possible for the six-atomic Cl + CH_4 system considering the above group of reactions.[6,13–16] In 2011, Czakó and Bowman[17] reported a full-dimensional *ab initio* potential energy surface (PES) and quasi-classical trajectory (QCT) simulations for the Cl + CH_4 reaction, which, for the first time, provided quantitative agreement between the computed and measured[5] HCl rotational distributions. In the past few years, first-principles dynamics have become possible for larger systems, such as the reactions of Cl with CH_3OH and C_2H_6 molecules.[11,12,18,19] In the case of Cl + C_2H_6, high-level *ab initio* analytical PES-based QCT computations performed in our group gave cold HCl rotational distributions,[19] again in excellent agreement with experiment,[2,3] thereby "resolving a nearly 25-year discrepancy with the experimental measurements."[20]

The present study extends the above-described line of research by investigating the dynamics of Cl with methylamine (CH_3NH_2) using first-principles theory. The HCl rotational distributions of the Cl + CH_3NH_2 reaction were measured[4] in 2003 as discussed by Murray and Orr-Ewing in the above-mentioned review article in 2004.[1] However, the theoretical studies of this reaction were restricted to stationary-point characterizations, rate coefficient determinations with a master equation model, and on-the-fly computations of a few trajectories.[4,21,22] In 2021, we also started to investigate the title reaction using high-level *ab initio* methods and,[23] unlike previous studies,[4,21,22] we reported benchmark stationary-point properties for several alternative product channels, such as methyl-, amino-, and hydrogen-substitution, besides two major hydrogen-abstraction pathways leading to HCl + CH_2NH_2/CH_3NH. Based on our previous work,[23] here we develop a full-dimensional global *ab initio* analytical PES for the eight-atomic Cl + CH_3NH_2 system using the ROBOSURFER program package[24] interfaced with MOLPRO[25] and the permutationally invariant polynomial fitting code.[26] The PES development for the title reaction is not just challenging because of its high dimensionality, but electronic structure problems, in particular Hartree–Fock (HF)[27] convergence issues, can occur in the entrance channel. We show how to overcome these *ab initio* difficulties by using our recently proposed ManyHF method,[28] whose use is found to be essential to obtain an accurate PES without applying multi-reference electronic-structure methods. The new PES enables us to perform efficient QCT simulations for the Cl + CH_3NH_2 reaction, allowing a direct comparison with previously measured HCl rotational distributions[4] as well as providing unprecedented insights into the dynamics of a new member of the Cl atom plus organic molecule reaction family.

In Sec. II, the details of the PES development are described, including the stationary-point characteristics, the selection of the initial geometries and their energy computations, the performance of the ManyHF method, as well as the details of the ROBOSURFER, the fitting, and the properties and accuracy of the analytical PES. The computational details of the QCT simulations are given in Sec. III, and the results are presented and discussed in Sec. IV. This paper ends with a summary and conclusions in Sec. V.

II. POTENTIAL ENERGY SURFACE

A. Characteristics of the PES

The first step of a full-dimensional analytical potential energy surface development is the mapping of the reaction pathways of the investigated process. The geometries and energies of the reactants, the most important transition states, the pre- and post-reaction complexes, and the products for six reaction channels of the Cl + CH_3NH_2 system were determined using a high-level *ab initio* method in our previous work.[23] Supplementing the unrestricted explicitly-correlated coupled-cluster singles, doubles, and perturbative triples (UCCSD(T)-F12b) aug-cc-pVQZ single-point energies obtained at the UCCSD(T)-F12b/aug-cc-pVTZ geometries with further energy contributions {δ[coupled-cluster singles, doubles, and triples (CCSDT)], δ[CCSDT(Q)], Δ_{core}, Δ_{rel}, Δ_{SO}, and Δ_{ZPE}} (see details in Ref. 23), the computations revealed that the low/submerged-barrier hydrogen abstractions from the two functional groups, leading to HCl + CH_2NH_2/CH_3NH, are exothermic on the vibrationally adiabatic potential energy surface. We denote the above hydrogen-abstraction (HA) channels as CH_3 HA/NH_2 HA. In order to obtain a comprehensive study of the title reaction and to prepare for the PES development, the hydrogen substitutions (H + CH_2ClNH_2/CH_3NHCl) and the functional-group substitutions (CH_3Cl + NH_2/CH_3 + NH_2Cl) were also scrutinized. Furthermore, we considered the Walden (W) inversion and the front-side (FS) attack mechanisms in the case of the amino-substitution (AS) and the methyl-hydrogen-substitution (CH_3 HS) pathways. Despite the fact that these are high-barrier, endothermic, chemically less-relevant pathways, reckon with the stationary points and products in these regions is required to develop a full-dimensional global PES. The classical (without Δ_{ZPE} correction) global minimum of the surface is a pre-reaction complex (PREMIN) in the entrance channel, and a post-reaction complex (CH_3 HA MIN″) in the product channel is the adiabatic global minimum, which can affect the reaction dynamics.

B. Initial geometry set

Based on the obtained highly accurate structures of the above-mentioned reaction pathways, the initial geometry set is constructed as follows: The Cartesian coordinates of the stationary points in the interaction region, reactants, and products are randomly displaced in the 0–0.32 Å range. Besides the displacements, the fragments of the reactants and products are scattered around each other in random orientations between the 2 and 8 Å distance. With this strategy, 500 geometries are generated in both the reactant and each product regions, while 250 random-displaced structures are created for each stationary point in the interaction region. In order to assemble an appropriate database of *ab initio* energy points for the PES development, single-point calculations are carried out for these geometries, where the UCCSD(T)-F12a method[29] is applied with the cc-pVDZ-F12 basis set.[30] Maintaining the balance between the computation demand and accuracy, basis set correction is taken into account using the restricted explicitly-correlated second-order Møller–Plesset perturbation method (RMP2-F12)[31] with both the cc-pVDZ-F12 and cc-pVTZ-F12 basis sets[30] providing high-level composite energies. During the evaluation of the relative energies, it was revealed that most of the results are converged to high-energy, excited electronic state(s) in the reactant region; hence, we applied the recently proposed ManyHF method[28] to solve this issue (detailed in Sec. II C). For the *ab initio* computations, the MOLPRO program package[25] is used and the energy points are determined as

$$\begin{aligned} E_{\mathrm{composite}} = {} & \text{ManyHF-UCCSD(T)-F12a/cc-pVDZ-F12} \\ & + (\text{ManyHF-RMP2-F12/cc-pVTZ-F12} \\ & - \text{ManyHF-RMP2-F12/cc-pVDZ-F12}). \end{aligned} \quad (1)$$

C. ManyHF vs default HF method

Since the correlation methods indicated in Eq. (1) use single-determinant HF wavefunctions as their reference, the composite energy can be inaccurate if the HF solution is a poor approximation of the exact ground-state wavefunction and/or HF converges to a wrong (excited) electronic state. In the case of the entrance-channel displaced geometries of the Cl + CH_3NH_2 system, the latter occurs many times, resulting in erratically high energies for the reactant region. The in-house ManyHF method[28] fixes this unreliability by choosing the lowest-energy HF reference for the correlation methods from various instances of HF calculations, where different sets of initial orbitals are applied. Recalculating the energy points with this pragmatic technique resulted in an excellent improvement in the accurate description of the reactant region. As Fig. 1 shows, where the absolute errors in the composite energy obtained with the default[25] and ManyHF approaches are displayed as a function of the ManyHF-based composite energy, these unacceptably high relative energies occur not only in the largely displaced geometry regions but in the near-equilibrium ones as well. However, in the case of the two hydrogen-abstraction product channels, the errors exceed 1 kcal mol^{-1} at only four cases from a total of 983 (where both methods give a composite energy). On the contrary, in the reactant channel, the errors are above 10 kcal mol^{-1} in the 0–20 kcal mol^{-1} region for 95.15% of the geometries. Moreover, the absolute difference between the potential energies obtained with the two approaches is below 1 kcal mol^{-1} for only 4.30% of the structures in the reactant region, as Table I shows, while for the other six cases (abstraction product, TS, and MIN regions), this difference is within 1 kcal mol^{-1} for more than 99% of the geometries. Besides the fact that the computations converge to the correct electronic state with the use of ManyHF, it is also obvious that the rate of successfully performed calculations increases (Table I). The previous reasons justify that the energy points are determined for the PES development using the ManyHF-based composite method.

TABLE I. Comparison of the success percentage of the default HF-based[25] and ManyHF-enhanced[28] quantum chemical computations for the regions of the reactants and the two hydrogen-abstraction pathways.

	Default HF (%)[a]	ManyHF (%)[b]	Identity (%)[c]
Cl + CH_3NH_2	73.20	94.60	4.30
HCl + CH_2NH_2	97.20	100.00	99.38
HCl + CH_3NH	99.40	100.00	99.80
CH_3 HA MIN	99.20	100.00	99.19
CH_3 HA TS	92.00	100.00	96.96
NH_2 HA MIN	100.00	100.00	99.60
NH_2 HA TS	97.20	99.60	99.17

[a] Percentage of the successfully completed default HF-based (with MOLPRO 2015.1)[25] composite energy calculations for the random displaced geometries.

[b] Percentage of the successfully completed ManyHF-based[28] composite energy calculations for the random displaced geometries.

[c] Percentage of the less than 1 kcal mol^{-1} absolute difference between the potential energy values obtained as a result of successfully executed calculations in both cases.

D. Potential energy surface development

After the single-point energy calculations at the random displaced geometries, the initial set contains 8693 components, which decrease to 7393 after the removal of the chemically irrelevant points, which have more than 200 kcal mol^{-1} energy relative to the global minimum of the set. The database is fitted with a fifth-order permutationally invariant polynomial.[26] Considering that the title Cl + CH_3NH_2 system contains five hydrogen atoms, it is expected to use a function that is invariant under the permutation of these H atoms. Therefore, a permutationally invariant full-dimensional extension of the $y_{ij} = \exp(-r_{ij}/a)$ Morse-like variables is used, where r_{ij} indicates the inter-atomic distances. The a parameter is set to 2.5 bohr, which controls the asymptotic behavior of the PES. The fitting coefficients are determined by a weighted linear least-squares fit, where each geometry is weighted with

$$w(E) = \frac{E_0}{E + E_0} \cdot \frac{E_1}{E + E_1}, \qquad (2)$$

where E is the potential energy of the geometry relative to the minimum of the dataset and E_0 and E_1 are set to 0.1 and 0.5 hartree, respectively. However, the resulting initial potential energy surface has a significant degree of inaccuracy; thus, the ROBOSURFER program package[24] developed in our research group is applied to handle this.

The concept of this program system is that the accuracy of the potential energy surface is improved by automatically adding

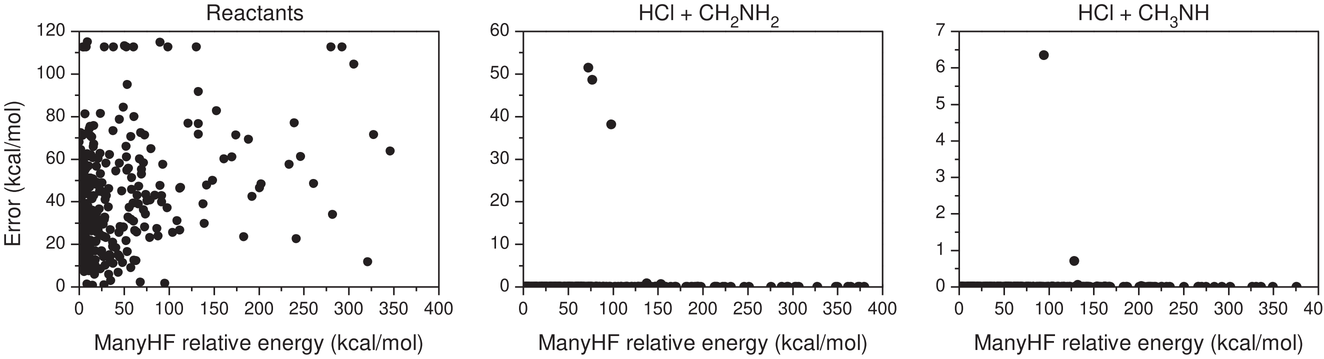

FIG. 1. Absolute errors of the default HF-based[25] composite energies as a function of the ManyHF-based[28] composite energies relative to the free reactants for the Cl + CH_3NH_2 entrance-channel geometries (left) and relative to the free products for the methyl (middle) and amino (right) hydrogen-abstraction pathways.

selected energy points to the fitting set, where the fitting error is above a threshold (E_{thresh}) set by the user. These new data points are extracted from QCT simulations during the development iteratively. In this work, these QCT computations are carried out at collision energies (E_{coll}) in the 10–80 kcal mol^{-1} range, where the increment is 10 kcal mol^{-1}. In each iteration at each E_{coll}, the trajectories are run at 0–8 bohr impact parameter with 0.5 bohr step and when the number of unphysical trajectories (which cannot be classified to any energetically available reaction channel) is decreased, the collision energy is increased and the next iteration is started. With this strategy, finally, the 74th version of the PES has been accepted to be the final, which contains 10 326 points.

As in the PES characterization article[23] reported in more detail, the energy lowering caused by the relativistic spin–orbit (SO) coupling must be taken into account for the title open-shell system in order to achieve chemical accuracy. The Davidson-corrected[32] all-electron multi-reference configuration interaction method[33] (MRCI+Q) is used combined with the aug-cc-pwCVDZ basis set[34] and applying the interacting-states approach.[35] During the MRCI computations, 5 electrons on 3 spatial 3p-like orbitals are used as an active space. The SO effect is calculated as the difference between the SO_1 and the non-SO_1 ground-state potential energies, i.e., $\Delta_{SO} = E_{SO1} - E_{\text{non-}SO1}$, and added to the single-point energies,

$$E_{\text{composite}} + \Delta_{SO}(\text{MRCI+Q}(5,3)/\text{aug-cc-pwCVDZ}). \tag{3}$$

In the case of 14 geometries, the multi-configurational self-consistent-field (MCSCF) method did not converge; therefore, the final coefficients forming the basis of the reaction dynamics simulations are determined on a dataset containing 10 312 points.

A measure of the potential energy surface quality is the root-mean-square (rms) error of the fitting, which is within the chemical accuracy in the most relevant region for this multi-channel reaction, since the rms values are 0.77, 1.45, and 2.29 kcal mol^{-1} at the 0.00–62.75, 62.75–125.50, and 125.50–313.75 kcal mol^{-1} intervals, respectively, which are defined relative to the global minimum of the dataset. (Note that the initial dataset was truncated at 200 kcal mol^{-1}, but during the ROBOSURFER iterations, higher-energy points were added even above 313.75 kcal mol^{-1}.) Meanwhile, the potential energies of the stationary points relative to the reactants are determined at the PES-optimized geometries and compared with the benchmark classical relative energies[23] (see Sec. II A), as shown in Fig. 2. Based on the rms values, the most accurate region of the PES is around −15 to 48 kcal mol^{-1}, relative to the reactants. Nevertheless, in the case of a few high-energy stationary points, the agreement of the benchmark and the PES values is excellent. For example, for the Walden-inversion transition state of the methyl hydrogen-substitution (CH_3 HS TS W) and amino-substitution (AS

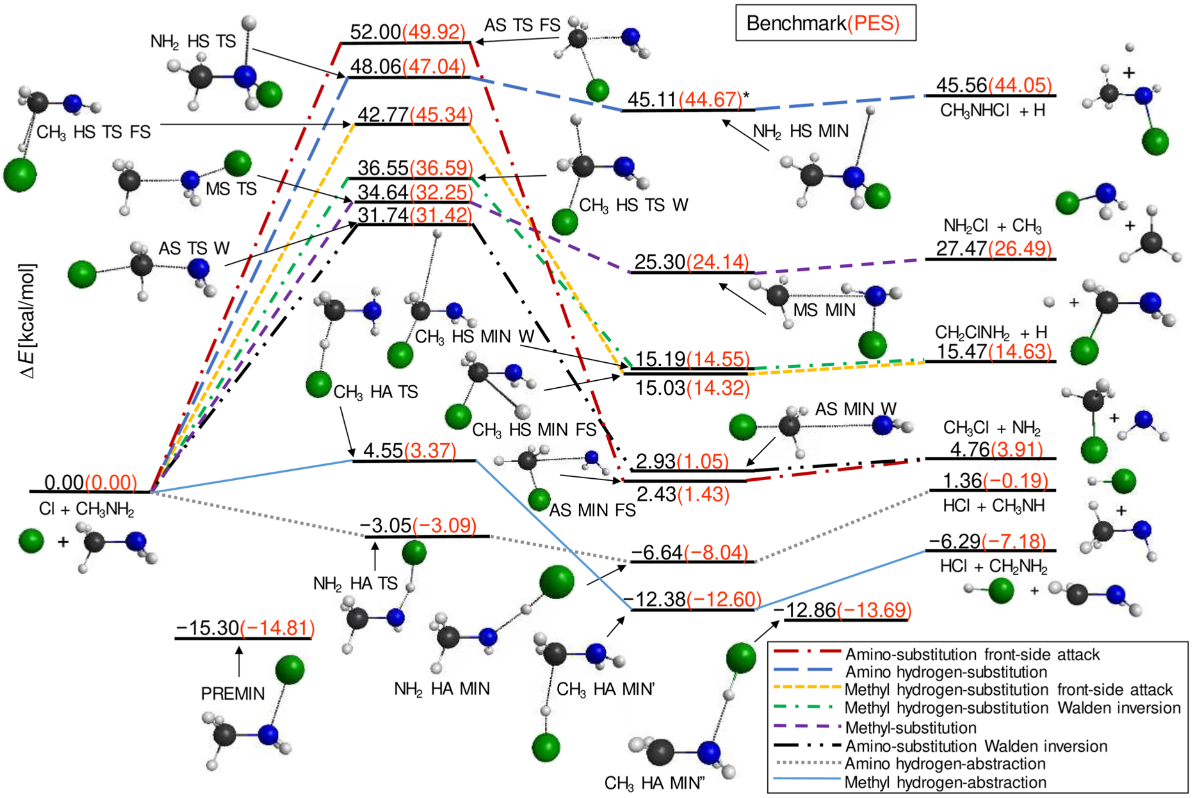

FIG. 2. Schematic potential energy diagram of the title reaction, where in addition to the CCSD(T)-F12b/aug-cc-pVTZ structures, the benchmark classical potential energies (detailed in Sec. II A, taken from Ref. 23) and the potential energies obtained at the newly developed PES-optimized geometries are shown relative to the reactants. The asterisk denotes the PES potential energy obtained at the CCSD(T)-F12b/aug-cc-pVTZ geometry. All energies are given in kcal mol^{-1}.

TS W) or the MIN complex of the amino hydrogen-substitution pathway (NH_2 HS MIN), the absolute differences are only 0.04, 0.32, and 0.44 kcal mol^{-1}, respectively. Furthermore, the PES describes within chemical accuracy the two structures with the deepest potential energy relative to the reactants, which may play a significant role in the dynamics: $|\Delta E_{PES} - \Delta E_{benchmark}| = 0.83$ and 0.49 kcal mol^{-1} for CH_3 HA MIN″ and PREMIN, respectively. Despite the fact that in some cases, the PES values have slightly larger deviations compared to the benchmark results, the absolute average deviation is 1.04 kcal mol^{-1} for all stationary points, which can be considered accurate for such a complex multi-channel reaction. Here, it is important to note that the comparison of the PES and the high-level benchmark energies shows the "absolute accuracy" of the PES and the deviations arise from both the fitting errors and the uncertainties of the *ab initio* level used for the PES development.

III. QUASI-CLASSICAL TRAJECTORY SIMULATIONS

On the newly developed potential energy surface, quasi-classical trajectory simulations are run. As ordinarily applied in the QCT method, at the beginning of the trajectories, the initial vibrational energy of the system is set to the ground vibration state by giving ZPE to the molecular reactant applying the normal-mode sampling.[36] The distance between the Cl atom and the CH_3NH_2 molecule is adjusted with the $\sqrt{x^2 + b^2}$ expression, where $x = 18.90$ bohr and b is the impact parameter. The latter is varied between 0.0 and b_{max} (or above) with 0.5 bohr steps at each $E_{coll} = 1$, 5, 10, 20, 30, 40, 50, and 60 kcal mol^{-1}, where b_{max} is reached when zero reaction probability occurs. The number of trajectories is 5000 at each E_{coll} and b. The trajectories are propagated with 0.0726 fs time step and stopped when the largest interatomic distance is higher than the initial largest one by 1 bohr.

IV. RESULTS AND DISCUSSION

The reaction dynamics results are obtained from the analysis of the trajectories of the QCT simulations. The first step of this investigation is the classification of each trajectory into reactive, non-reactive, or unphysical categories; moreover, the reactive ones are assigned to the appropriate reaction channels. Unphysical means that the reaction cannot be classified as either reactive or non-reactive, i.e., energetically not allowed products are obtained. (The number of unphysical trajectories is negligible in the collision energy range of 1–60 kcal mol^{-1}.) Representing the reaction probability as a function of the b impact parameter gives the opacity function [$P(b)$], and the b-weighted numerical integration of this provides the integral cross section (σ) data. Based on the latter, the two hydrogen-abstraction pathways are selected for a more detailed investigation since the other channels have negligible σ against these two. The H-substitution from the methyl-group, the amino-substitution channel, and the H-substitution from the amino-group open at $E_{coll} = 30$, 40, and 60 kcal mol^{-1}, respectively, but at the highest 60 kcal mol^{-1} collision energy used in our simulations, the σ is only 0.0405, 0.0082, and 0.0003 $bohr^2$ for these cases. Meanwhile, the two abstraction pathways occur at all collision energies used for the simulations in this work and the cross section values are significant as well, see below. Therefore, in the following, the results are reported only for the reactions resulting in the HCl + CH_2NH_2/CH_3NH products, including the attack and scattering angle distributions, the post-reaction distributions of energy, and the rotational quantum number (J) distributions of the HCl product. For the latter and for the integral cross sections (ICSs), soft and hard ZPE constraints are applied, where the following conditions must be fulfilled for the vibrational energy and ZPE of products in order not to reject a trajectory:

$$\text{Soft: } E_{vib}(CH_2NH_2) + E_{vib}(HCl) > ZPE(CH_2NH_2) + ZPE(HCl) \quad (CH_3\ HA), \tag{4}$$

$$E_{vib}(CH_3NH) + E_{vib}(HCl) > ZPE(CH_3NH) + ZPE(HCl) \quad (NH_2\ HA), \tag{5}$$

$$\text{Hard: } E_{vib}(CH_2NH_2) > ZPE(CH_2NH_2) \quad \text{and} \quad E_{vib}(HCl) > ZPE(HCl) \quad (CH_3\ HA), \tag{6}$$

$$E_{vib}(CH_3NH) > ZPE(CH_3NH) \quad \text{and} \quad E_{vib}(HCl) > ZPE(HCl) \quad (NH_2\ HA). \tag{7}$$

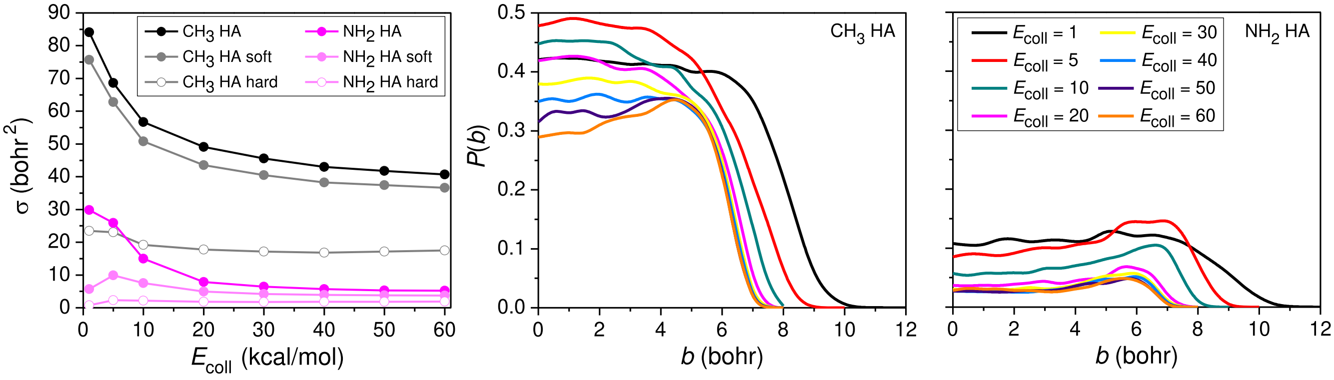

FIG. 3. Integral cross sections as a function of the collision energy for the two functional-group hydrogen abstractions for the Cl + CH_3NH_2 reaction, with and without zero-point energy restrictions (left). Reaction probabilities as a function of the impact parameter at eight different collision energies, given in kcal mol^{-1}, for the methyl hydrogen-abstraction channel (middle) and for the amino hydrogen-abstraction channel (right).

In the soft case, the trajectory is taken into account if the sum of the zero-point energies of the products has a smaller value than the sum of their vibrational energies. These conditions must be valid for each product separately in order for the trajectory to be acceptable in the hard approach.

A. Integral cross sections and opacity functions

The opacity functions are represented in Fig. 3 at the eight collision energies (1, 5, 10, 20, 30, 40, 50, and 60 kcal mol^{-1}) applied in the QCT simulations. It is obvious that the hydrogen abstraction occurs more frequently from the methyl group, which is expected from the thermodynamic conditions, since this is an exothermic pathway, and from the statistics due to the number of hydrogens. For example, the reaction probability of the methyl H-abstraction is 14.0 times higher than the amino H-abstraction at 30 kcal mol^{-1} collision energy and 1 bohr impact parameter and 14.4 times at 40 kcal mol^{-1} and b = 2 bohr. These ratios are slightly large especially that CH_3 HA has a ~4 kcal mol^{-1} barrier, while the NH_2 HA is a submerged-barrier pathway. The lower reactivity of the NH_2 hydrogens can be explained by the non-bonding electron pair of the nitrogen atom, which steers the reaction to the non-reactive PREMIN complex in the entrance channel, where the chlorine atom binds to the methylamine from the amino-group. The maximum value of b ($b_{\max}$, where the probability vanishes) decreases as the collision energy increases from about 10 to 7 bohr in both cases in accordance with the presence of long-range interactions, which can prevail at low collision energies. The impact parameter generally affects the shape of the curves in the way that the probability does not change significantly in the 0–6 bohr interval and then abruptly drops. However, instead of a near constant phase, peaks close to the $b_{\max}$ value are formed as the collision energy increases, which indicates a mechanism shifting to the direct stripping, which can be seen as well in the later discussed scattering angle distributions and translational energy distributions.

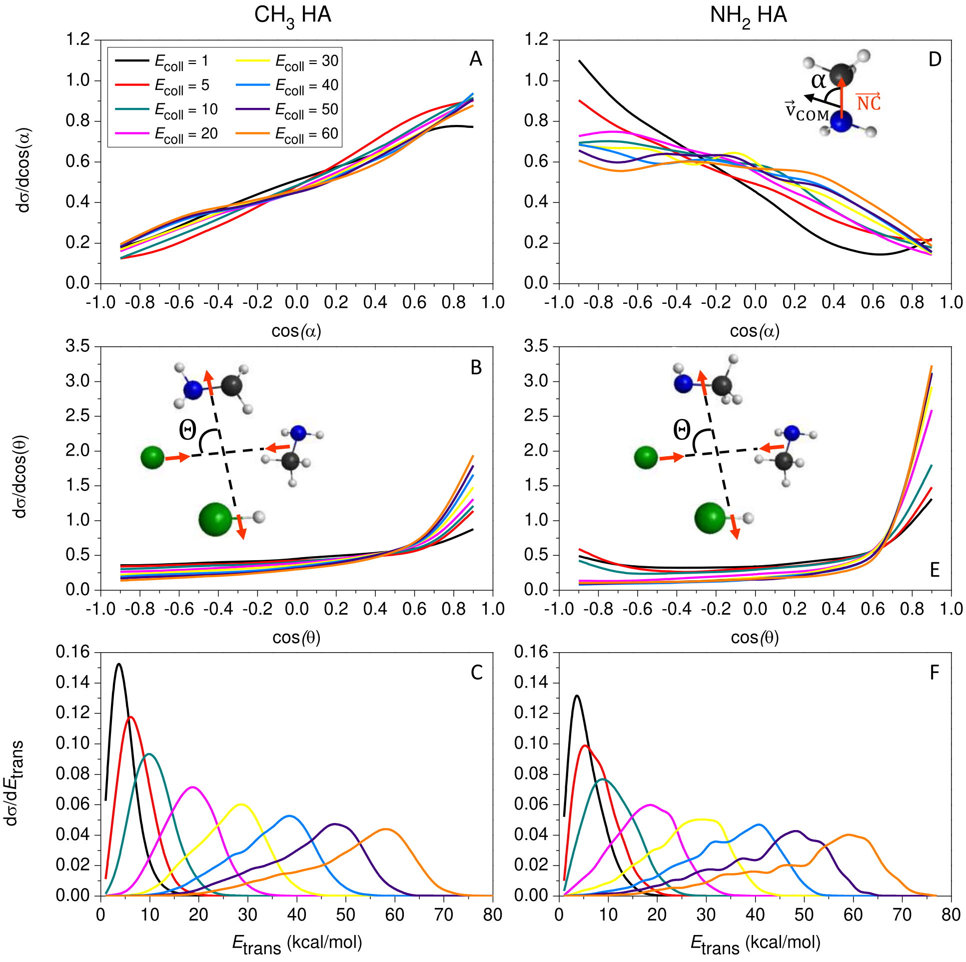

FIG. 4. Normalized initial attack angle (first row), scattering angle (second row), and product relative translational energy (third row) distributions of hydrogen-abstraction from the methyl group (a)–(c) and amino group (d)–(f) at eight different collision energies (kcal mol^{-1}).

Integral cross sections as a function of the collision energy are shown in Fig. 3 as well, considering the ZPE constraints defined by Eqs. (4)–(7). The preference of the methyl hydrogen-abstraction pathway can also be seen here because without the restrictions at 1 kcal mol^{-1} collision energy, the σ is 84.07 bohr^2 for this channel and 29.86 bohr^2 for the abstraction from the amino-group, and the σ is 40.69 and 5.20 bohr^2, respectively, at E_{coll} = 60 kcal mol^{-1}. Note that the experiment found almost equal reactivity for the two hydrogen-abstraction channels at E_{coll} of ~5 kcal mol^{-1},[4] whereas the present simulations show an enhancement of CH_3 HA relative to NH_2 HA by a factor of 2.65 at this E_{coll}. With increasing collision energy, the ICS is decreasing for both reaction channels. For the amino-hydrogen substitution pathway, this is expected since the relative energy of the stationary points is below the reactants. However, for the other reaction where a slightly low positive barrier exists, this behavior may be explained by the artifacts of the classical simulations, where the ZPE can flow between the vibrational modes whose effects may allow reactivity at lower collision energies than the adiabatic barrier height. Nevertheless, it is important to note that future quantum dynamics computations, where tunneling can facilitate reactivity at low E_{coll}, may support the decaying excitation function. The decrease in the ICS caused by the soft constraint is around 10% for the CH_3 abstraction, which increases to ~70% for the hard case at low collision energies and ~60% at high collision energies. The ZPE violation is more significant at low collision energies for the NH_2 abstraction pathway, as it can be seen that the constrained ICS is less than the no-constraint data by 81.63% and 97.49% at E_{coll} = 1 kcal mol^{-1} in the soft and hard cases, respectively,

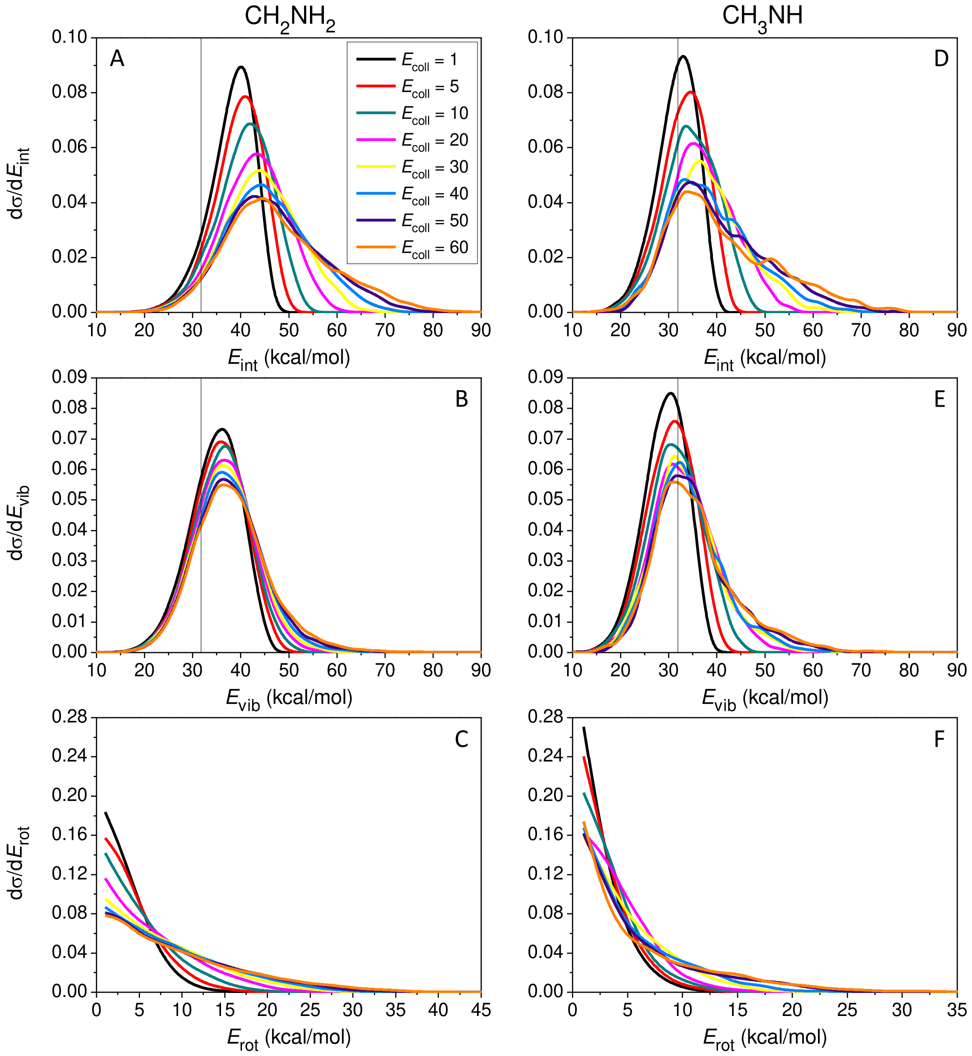

FIG. 5. Normalized internal (first row), vibrational (second row), and rotational (third row) energy distributions of the CH_2NH_2 product formed by hydrogen-abstraction from the methyl group (a)–(c) and of the CH_3NH product formed by amino-hydrogen abstraction (d)–(f) at eight different collision energies (kcal mol^{-1}). Vertical lines indicate the zero-point energy values of the molecules.

whereas these effects are only 28.35% and 63.22% at E_{coll} = 60 kcal mol^{-1}.

B. Attack angle, scattering angle, and product relative translational energy distributions

The initial attacking orientation leading to the hydrogen-abstraction reactions is investigated by the examination of the angle (α) of the center of mass velocity vector of the reactant molecule and the interatomic N–C vector. As Fig. 4 shows, the cosine of the α values is assigned to one of ten bins equidistant in the −1 to 1 range. The inserted figure of the methylamine visualizes that if α equals to 0° [cos(α) = 1], the chlorine approaches the molecule from the CH_3 group side in line with the C–N bond and Cl approaches CH_3NH_2 from the NH_2 group side when α = 180° [cos(α) = −1]. Differential cross sections (DCSs) as a function of cos(α) show directional preferences, as the reactant atom abstracts the hydrogen from that functional group wherefrom the chlorine attacks. The attack-angle distribution of NH_2 HA [Fig. 4(d)] has more significant collision-energy dependence than the other pathway [Fig. 4(a)]. At higher E_{coll}, the distribution is more isotropic, as the decrease in the DCS is modest in the −1 to 0 range, indicating that side-on attack can occur as well; despite this at E_{coll} = 1 and 5 kcal mol^{-1}, the descent is more rapid.

The scattering angle (θ) is defined as the angle of the relative velocity vectors of the center of masses of the products and reactants. The binning of the cosine θ is implemented as previously described for cosine α (ten bins in the −1 to 1 range). The θ = 0° case [cos(θ) = 1] corresponds to the forward-scattering, and θ = 180° [cos(θ) = −1] defines the backward-scattering. With increasing collision energy, the mechanism shifts to direct stripping more and

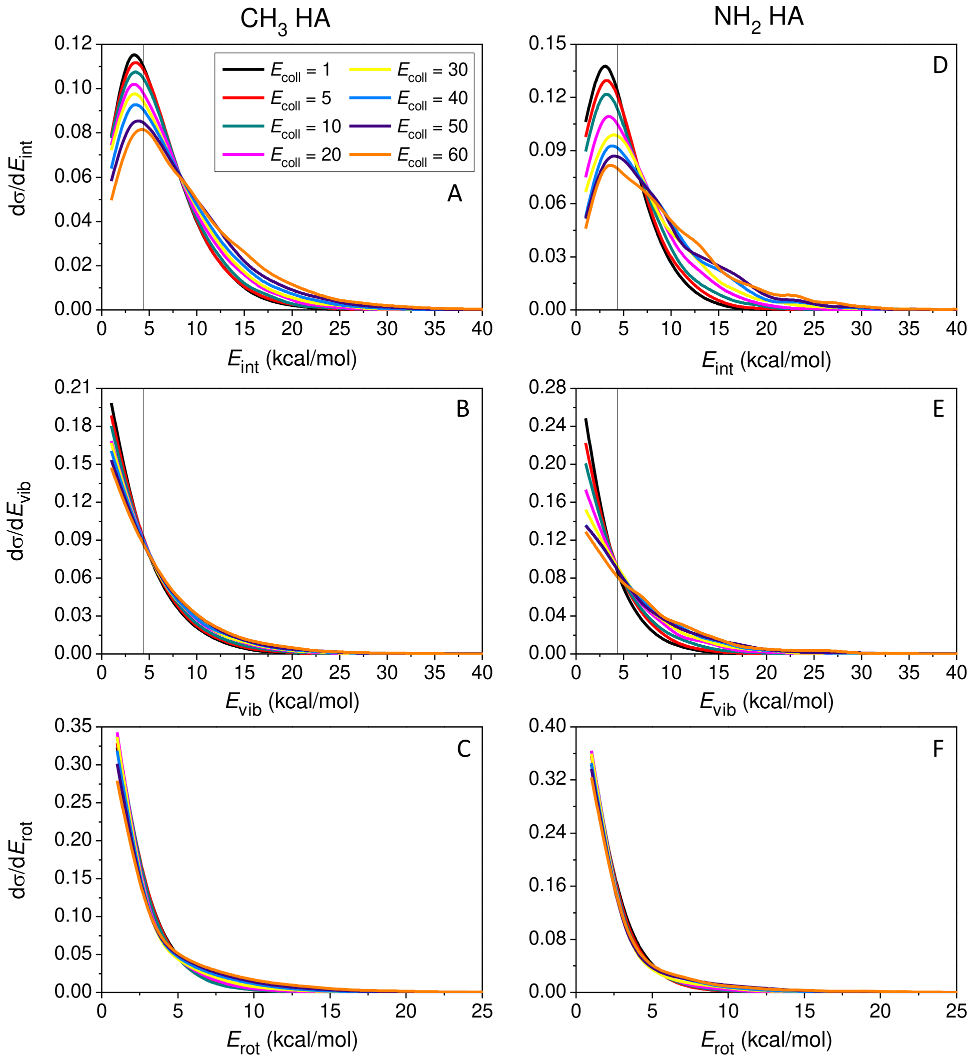

FIG. 6. Normalized internal (first row), vibrational (second row) and rotational (third row) energy distributions of HCl formed by hydrogen-abstraction from the methyl group (a)–(c) and from the amino-group (d)–(f) at eight different collision energies (kcal mol^{-1}). The vertical lines indicate the zero-point energy value of the HCl molecule.

more for both channels, where the forward-scattering occurs [see Figs. 4(b) and 4(e)], in consistent with the statements expressed for the reaction probabilities. This mechanism is also preferred at lower E_{coll}, but the scattering is more isotropic in these cases, which indicates indirect characteristic at low collision energies especially in the case of abstraction from the methyl group, where a prolonged rise in the shape of the curves can be seen.

The relative translational energy (E_{trans}) distributions of the reaction products (HCl + CH_2NH_2/CH_3NH) at the eight collision energies used for simulations are investigated as well [Figs. 4(c) and 4(f)]. The maximum of the curves appears where the E_{trans} is around the applied collision energy, which reveals an efficient translational energy transfer from the reactants to the products. The plotted cross sections show that the peak of the curves drifts from the lower E_{trans} forward to higher E_{trans} with increasing collision energy. This supports our claims about the mechanism shifting from the indirect to the direct since during the former, complexes are formed and the separated products have less translational energy than in the case of the direct reaction.

C. Internal, vibrational, and rotational energy distributions

The collision energy set at the beginning of the simulations can transfer to the relative translation of the products, as described above, or to the products' internal degrees of freedom. The internal energy (E_{int}) can be separated into vibrational (E_{vib}) and rotational (E_{rot}) parts using a classical rigid rotor approximation for E_{rot}, and then, E_{vib} is obtained as $E_{\mathrm{int}} - E_{\mathrm{rot}}$. In the case of the title reaction, the internal energy transfer is less efficient than the translational as it can be seen in Figs. 5 and 6 since the internal energies that correspond to the peaks are in a narrow interval for all E_{coll} values and do not change with E_{coll} as much as in the case of E_{trans}. The internal energy distributions of the CH_2NH_2 product [Fig. 5(a)] are clearly hotter (peaks are in the 40–45 kcal mol^{-1} range) than those of CH_3NH [peaks are in the 33–35 kcal mol^{-1} range; see Fig. 5(d)], and the ZPE violation is less significant, which is expected as the methyl-hydrogen abstraction is a more exothermic reaction channel. Moreover, the shape of the curves changes more

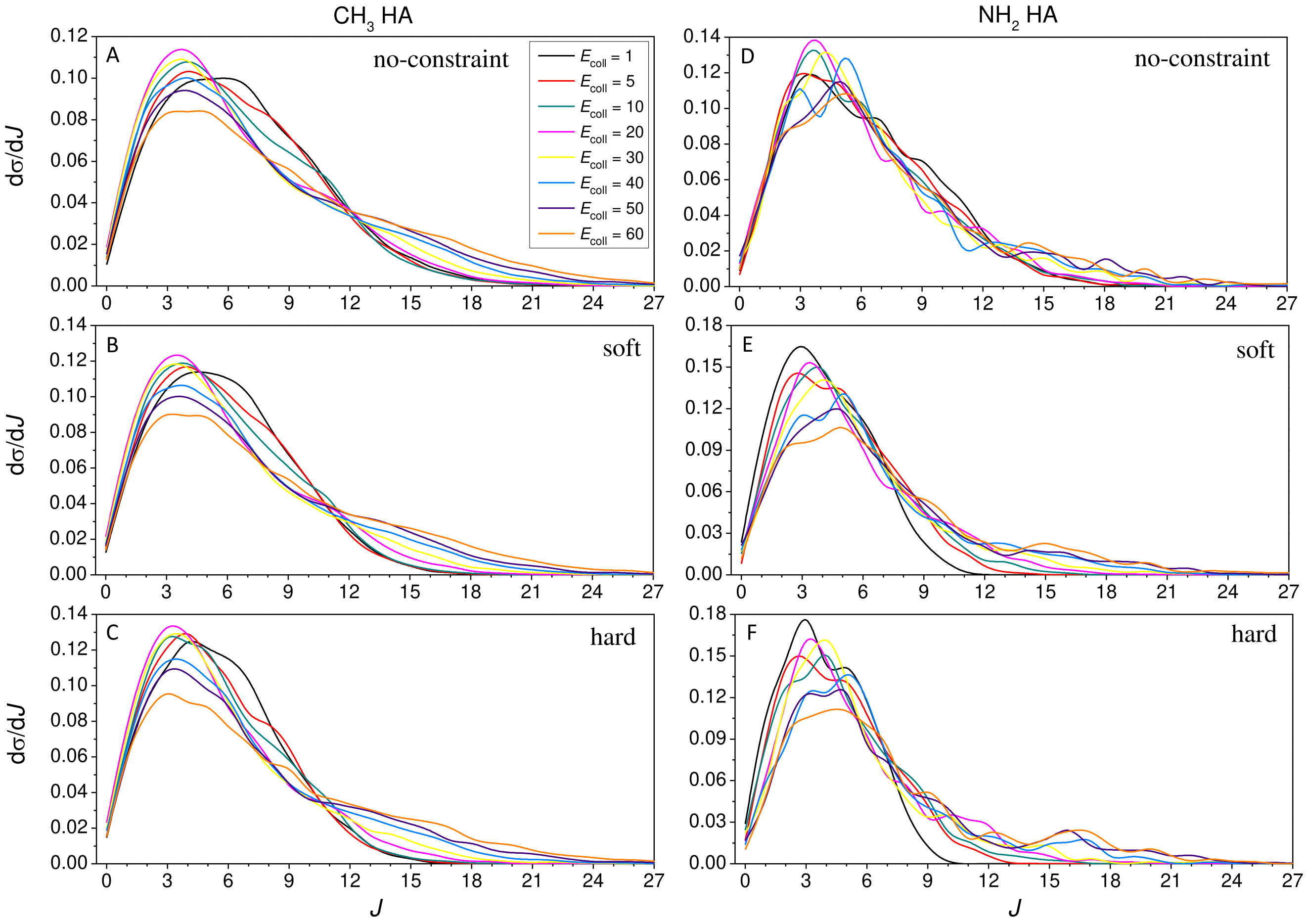

FIG. 7. Normalized rotational quantum number (*J*) value distributions for the HCl product originating from the methyl-hydrogen abstraction (a)–(c) and amino-hydrogen abstraction (d)–(f) without ZPE constraint (first row), with soft (second row) and hard (third row) constraints at eight collision energies (kcal mol^{-1}).

with the collision energy increase for CH_2NH_2 than for CH_3NH, which originates from the rotational energy of the molecule. In the case of these two molecules, the vibrational energy [Figs. 5(b) and 5(e)] is much hotter than the rotational energy [Figs. 5(c) and 5(f)], in contrast to the HCl vibrational and rotational distributions, which have a fairly similar scale. The zero-point energy of the HCl molecule is 4.32 kcal mol^{-1} (obtained on the PES), which is comparable with the internal energy corresponding to the highest DCS values, resulting in significant ZPE violation (see Fig. 6), which can be explained by the moderate exothermicity of these reaction channels.

D. Rotational quantum number value distributions

The rotational quantum number (J) values are determined for the product HCl of the amino- and methyl-hydrogen abstraction channels at the eight collision energies as well. The soft and hard ZPE constraints are also taken into account, and the normalized distributions are plotted in Fig. 7. The difference between the CH_3 HA [Figs. 7(a)–7(c)] and the NH_2 HA [Figs. 7(d)–7(f)] plots is slight since the most populated levels are J = 3–6 for both channels, but for the methyl-group reaction, the distributions are smoother due to the better statistical accuracy. With the rejection of the ZPE-violating trajectories, the curves decay more rapidly for both cases. Applying selective deuteration, experiments suggest that CH_3 HA results in rotationally hotter HCl products than NH_2 HA,[4] which is not confirmed by the present simulations. Nevertheless, the computed CH_3-site specific HCl distributions agree well with experiment, and the difference is in the NH_2 HA results, where the measured distribution is significantly colder.

In this study, non-constrained, soft and hard distributions of the J values for the ground vibrational state (v = 0) of HCl are investigated without distinguishing the two hydrogen-abstraction pathways in order to directly compare our data with the experimental results measured by Orr-Ewing and co-workers.[4] In Fig. 8, the experimental and theoretical values are represented together, where the latter results are obtained at E_{coll} = 5 kcal mol^{-1}. The normalization is performed from J = 0 to 8 due to the limits in the experimental signal-to noise ratio; however, as we described above (Fig. 7), higher J levels exist. The distributions determined in this work are shifted toward higher rotational quantum numbers in contrast to the experimentally obtained results. The measured HCl(J) distribution of the title reaction is similar (peak at J = 1) to, albeit slightly hotter than, that of Cl + CH_4/C_2H_6;[2,3,5] however, the present agreement between theory and experiment is surprisingly not as impressive as in the case of the Cl + CH_4/C_2H_6 systems,[17,19] even if the applied level of theory is basically the same. Nevertheless, it is important to note that based on the site-specific results discussed above, theory and experiment are in good agreement for the CH_3 HA channel and the contradiction arises from the NH_2 site. To quantitatively support this conclusion, we have computed the average rotational energy of the HCl(v = 0) product at E_{coll} = 5 kcal mol^{-1}, which is 2.08, 1.85, and 2.01 kcal mol^{-1} in the case of CH_3-, NH_2-, and no site specificity, respectively, in reasonable agreement with the measured CH_3-specific energy (1.43 kcal mol^{-1}) and substantially overestimating the NH_2- (0.35 kcal mol^{-1}) and non-specific (0.65 kcal mol^{-1}) experimental data.[4]

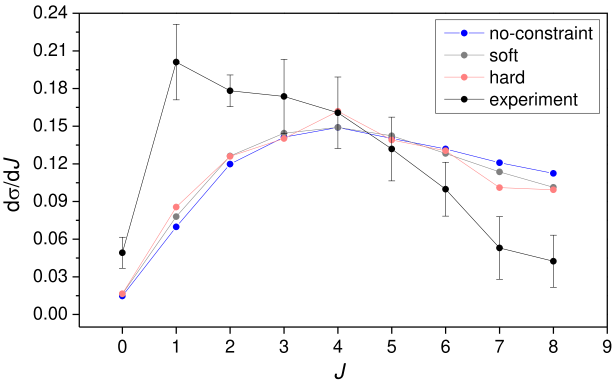

FIG. 8. Theoretical (E_{coll} = 5 kcal mol^{-1}) and experimental[4] normalized rotational quantum number (J) value distributions (non-site-specific) for the v = 0 vibrational state of the HCl product originating from the two hydrogen-abstraction pathways.

V. SUMMARY AND CONCLUSIONS

Based on our previous *ab initio* mapping of the potential energy surface of the multi-channel Cl + CH_3NH_2 reaction,[23] automated full-dimensional PES development is performed using the ROBOSURFER program system[24] and the permutationally invariant polynomial method.[26] We have found that a HF convergence issue in the entrance channel makes the PES development practically impossible with default settings in MOLPRO 2015.1;[25] however, our in-house ManyHF method[28] provides a solution to the problem, allowing accurate *ab initio* computations with a single-reference method. Thus, the fitted energy points used for the PES development are computed with a high-level ManyHF-based coupled-cluster-quality composite energy approach and the final fitting set is complemented with spin–orbit correction. The newly developed potential energy surface describes the stationary points of the reaction pathways with appropriate accuracy opening the door to quasi-classical trajectory simulations. From the analysis of the QCT results, it turns out that the most reactive channels are the hydrogen-abstractions from the functional-groups leading to the HCl + CH_2NH_2/CH_3NH products; hence, the more detailed reaction dynamics investigations are carried out for these channels. Besides the fact that the preference of the methyl-hydrogen abstraction is revealed, the integral cross sections show that both reactions have exothermic barrier-less characteristics and the ZPE violation is significant, especially with the hard constraint in the CH_3 HA case. With the reaction probability representation as a function of the impact parameter, the dominance of the direct stripping mechanism at high collision energies is uncovered and supported by the scattering angle and translational energy distributions of the products. The methyl-side attack of the chlorine atom is favored for the methyl-hydrogen abstraction, and if Cl approaches the methylamine from the opposite direction, the hydrogen of the product HCl mainly originates from the amino-group, as it is expected and verified by the initial angle distributions. As from the post-reaction energy distributions can be seen, the energy transfer from the reactants to the relative translational energy of the products is more efficient than to their internal energy. The vibrational and rotational energies of HCl can be assigned to similar scales, which cannot be claimed about the co-products. In addition, the E_{vib} and E_{rot} distributions of the co-products CH_2NH_2/CH_3NH show more significant collision-energy dependence. In the case of the HCl product, the rotational quantum number (J) value distributions are determined with no-, soft, and hard ZPE constraints; moreover, the values (assigned to $v = 0$) obtained at $E_{\mathrm{coll}} = 5$ kcal mol^{-1} are compared to the experimental data. Despite the similar methodology, the agreement between theory and experiment is not as good in the present case than for the Cl + CH_4/C_2H_6 systems, warranting future investigations on the dynamics of the title reaction.

SUPPLEMENTARY MATERIAL

See the supplementary material for PES codes (Ref. 26).

ACKNOWLEDGMENTS

We acknowledge the National Research, Development and Innovation Office (NKFIH), Grant No. K-125317, Project No. TKP2021-NVA-19, provided by the Ministry of Innovation and Technology of Hungary from the National Research, Development and Innovation Fund, financed under the TKP2021-NVA funding scheme, and the Momentum (Lendület) Program of the Hungarian Academy of Sciences for financial support.

AUTHOR DECLARATIONS

Conflict of Interest

The authors have no conflicts to disclose.

Author Contributions

Tímea Szűcs: Data curation (lead); Formal analysis (lead); Investigation (lead); Methodology (equal); Validation (equal); Visualization (lead); Writing – original draft (lead); Writing – review & editing (equal). **Gábor Czakó**: Conceptualization (lead); Data curation (supporting); Formal analysis (supporting); Funding acquisition (lead); Investigation (supporting); Methodology (equal); Project administration (lead); Supervision (lead); Validation (equal); Visualization (supporting); Writing – original draft (supporting); Writing – review & editing (equal).

DATA AVAILABILITY

The data that support the findings of this study are available from the corresponding author upon reasonable request.

REFERENCES

[1] C. Murray and A. J. Orr-Ewing, Int. Rev. Phys. Chem. **23**, 435 (2004).

[2] S. A. Kandel, T. P. Rakitzis, T. Lev-On, and R. N. Zare, J. Chem. Phys. **105**, 7550 (1996).

[3] S. Rudić, D. Ascenzi, and A. J. Orr-Ewing, Chem. Phys. Lett. **332**, 487 (2000).

[4] S. Rudić, C. Murray, J. N. Harvey, and A. J. Orr-Ewing, Phys. Chem. Chem. Phys. **5**, 1205 (2003).

[5] C. Murray, B. Retail, and A. J. Orr-Ewing, Chem. Phys. **301**, 239 (2004).

[6] J. F. Castillo, F. J. Aoiz, and L. Bañares, J. Chem. Phys. **125**, 124316 (2006).

[7] S. J. Greaves, R. A. Rose, F. Abou-Chahine, D. R. Glowacki, D. Troya, and A. J. Orr-Ewing, Phys. Chem. Chem. Phys. **13**, 11438 (2011).

[8] S. Rudić, C. Murray, J. N. Harvey, and A. J. Orr-Ewing, J. Chem. Phys. **120**, 186 (2004).

[9] S. J. Greaves, J. Kim, A. J. Orr-Ewing, and D. Troya, Chem. Phys. Lett. **441**, 171 (2007).

[10] S. J. Greaves, A. J. Orr-Ewing, and D. Troya, J. Phys. Chem. A **112**, 9387 (2008).

[11] C. Rangel and J. Espinosa-Garcia, Phys. Chem. Chem. Phys. **20**, 3925 (2018).

[12] J. Espinosa-Garcia, E. Martinez-Nuñez, and C. Rangel, J. Phys. Chem. A **122**, 2626 (2018).

[13] C. Rangel, M. Navarrete, J. C. Corchado, and J. Espinosa-García, J. Chem. Phys. **124**, 124306 (2006).

[14] D. Troya and P. J. E. Weiss, J. Chem. Phys. **124**, 074313 (2006).

[15] S. T. Banks and D. C. Clary, Phys. Chem. Chem. Phys. **9**, 933 (2007).

[16] S. M. Remmert, S. T. Banks, J. N. Harvey, A. J. Orr-Ewing, and D. C. Clary, J. Chem. Phys. **134**, 204311 (2011).

[17] G. Czakó and J. M. Bowman, Science **334**, 343 (2011).

[18] D. Lu, J. Li, and H. Guo, CCS Chem. **2**, 882 (2020).

[19] D. Papp, V. Tajti, T. Győri, and G. Czakó, J. Phys. Chem. Lett. **11**, 4762 (2020).

[20] T. P. Rakitzis, Science **371**, 886 (2021).

[21] M. S. Taylor, S. A. Ivanic, G. P. F. Wood, C. J. Easton, G. B. Bacskay, and L. Radom, J. Phys. Chem. A **113**, 11817 (2009).

[22] J. M. Nicovich, S. Mazumder, P. L. Laine, P. H. Wine, Y. Tang, A. J. C. Bunkan, and C. J. Nielsen, Phys. Chem. Chem. Phys. **17**, 911 (2015).

[23] T. Szűcs and G. Czakó, Phys. Chem. Chem. Phys. **23**, 10347 (2021).

[24] T. Győri and G. Czakó, J. Chem. Theory Comput. **16**, 51 (2020).

[25] H.-J. Werner, P. J. Knowles, G. Knizia, F. R. Manby, M. Schütz *et al.*, MOLPRO, Version 2015.1, a package of *ab initio* programs, 2015, http://www.molpro.net.

[26] B. J. Braams and J. M. Bowman, Int. Rev. Phys. Chem. **28**, 577 (2009).

[27] W. J. Hehre, L. Radom, P. v. R. Schleyer, and J. A. Pople, *Molecular Orbital Theory* (Wiley, New York, 1986).

[28] T. Győri and G. Czakó, J. Chem. Phys. **156**, 071101 (2022).

[29] G. Knizia, T. B. Adler, and H.-J. Werner, J. Chem. Phys. **130**, 054104 (2009).

[30] K. A. Peterson, T. B. Adler, and H.-J. Werner, J. Chem. Phys. **128**, 084102 (2008).

[31] G. Knizia and H.-J. Werner, J. Chem. Phys. **128**, 154103 (2008).

[32] S. R. Langhoff and E. R. Davidson, Int. J. Quantum Chem. **8**, 61 (1974).

[33] K. R. Shamasundar, G. Knizia, and H.-J. Werner, J. Chem. Phys. **135**, 054101 (2011).

[34] K. A. Peterson and T. H. Dunning, Jr., J. Chem. Phys. **117**, 10548 (2002).

[35] A. Berning, M. Schweizer, H.-J. Werner, P. J. Knowles, and P. Palmieri, Mol. Phys. **98**, 1823 (2000).

[36] W. L. Hase, *Encyclopedia of Computational Chemistry* (Wiley, New York, 1998), pp. 399–407.